Chapter 2

Optical Fiber Probe-Based Manipulation of Cells

Xiaoshuai Liu and Yao Zhang

Abstract

In a liquid environment, optical trapping and multifunctional manipulation of biological cells, in a noncontact, noninvasive, and high-precision way, have become one of the research focuses in the field of integrated optics, biophotonics, and clinical medicine. However, it still faces great challenges to perform multifunctional manipulation in very narrow spaces with high flexibility, including stable retaining, controllable deformation, and precise regulation of a cell chain. Therefore, in this chapter, we introduce the multifunctional manipulation for biological cells based on the elaborately designed fiber probes. With the probes, the sequential organization, precise regulation, and bidirectional transportation of the cell chain were performed. We also discuss the potential applications of fiber probes on the endocytosis and exocytosis purpose, which will play an important role in the detection and treatment of complex disease.

Keywords: optofluidic manipulation, fiber probe, cell chain, biophotonics, fiber tweezers

1. Introduction

In the field of endocytosis and exocytosis, a precise manipulation of a cell was required, especially for the nanomedicine injection, intracellular signaling pathway, and pathogenic research, which holds a great potential in the detection and treatment of complex diseases [1]. Thus, increasing attentions have been paid to the dynamic manipulation of cells in a fluid, which has been proved to be crucial in cell growth [2, 3], differentiation [4–6], drug delivery [7–9], mechanical force transduction [10, 11], etc. Up to now, diverse techniques have shown invaluable performance in the multifunctional manipulation of cells, including dielectrophoretic [12, 13], magnetic field [14, 15], and mechanical force [4, 16, 17]. Nevertheless, these strategies face the challenges of potential sample heating and high power consumption and required attachment of electric/magnetic nanoparticles [18, 19]. Besides, the cells were required to be confined on an elaborated substrate, which was usually not reusable in these techniques [20, 21].

Since first introduced by A. Ashkin, optical tweezers have motivated many intriguing advances in interdisciplinary applications, such as micro/nanophotonics, biphotonics, and biomedicine [22–24]. The most commonly used optical manipulation tool is the conventional optical tweezers (COTs), which uses high numerical aperture objectives to focus the free-space laser beam [25, 26]. After the transfer of photon momentum, the cell will suffer from the optical force, which can be

divided into optical scattering force and gradient force, with the direction pointed to the optical propagating direction and beam focus, respectively. The magnitude of optical force was ranged from femtonewton to nanonewton, and thus, it was the ideal chose to measure the response of biological and macromolecular system [27]. Compared to other microscopic techniques, for example, electric filed, magnetic field, and acoustic method, optical tweezers have the great potential of high precision, high flexibility, noncontact, and wide manipulation range. However, COTS faces certain challenges, such as bulky structure, limited integration, and diffraction for nanoparticles [28]. Thus, researchers have developed various schemes of optical tweezers to extend the potential application scenario, including holographic optical tweezers (HOTs), surface plasmon-based optical tweezers (SPOTs), and fiber probe-based optical tweezers (FP).

For HOTs, the optical tweezer system was inserted with a diffractive beam splitter. Then the beam wavefront can be further sculptured, which can manipulate multiple cells simultaneously [29–31]. Nevertheless, appropriate algorithms are required to be elaborately designed for achieving a specific pattern of cells. In addition, the complicated optical system was consisted of dichroic mirrors, spatial light modulators, and high-numerical-aperture focusing objectives. The working distance of objectives limits the depth at which cells can be manipulated in the cell suspensions. Besides HOTs, surface plasmon-based optical tweezers (SPOTs) have also been developed to manipulate cells with high trapping stability and retaining ability, especially for the sub-microsized cells and biological molecules [32, 33]. However, once the substrates designed, the cell pattern is fixed without a flexibility to adjust and transport the cell chain dynamically. Moreover, the organization of cell pattern is also limited at a specific depth of cell suspension. Thus, there is a great need of developing a new strategy to perform the multifunctional manipulation of cells.

2. Fiber probe-based optical tweezers

First, we will give a detailed introduction about the fiber probe-based optical tweezers. As for optical tweezers, a focused laser beam was essential for the stable trapping and dynamic manipulation of cells. To realize a focused laser beam, the fiber probe was designed into a tapered tip, for which the laser beam will be focused by the paraboloid end. After one cell approached the beam focus, it will suffer from the optical gradient force and then attracted into the optical axis. After that, it will be pushed away from the probe tip or attracted into the focus, which depends on the struggling of optical scattering force and gradient force along the optical axis direction. After the cell was trapped one by one, a specific organization of cell pattern can be achieved with the fiber probe. Further, the organized cell pattern can be shifted dynamically in the three dimensional direction. The FPs were fabricated by drawing commercial single-mode optical fibers with a flame-heating technique. By adjusting the stretch parameters, various parabolic ends can be achieved to conduct the multifunctional manipulation of the cell. With the high flexibility, ease fabrication, and compact size, fiber probe-based optical tweezers have been widely used for the trap of dielectric microparticles and cells [28], the shift of fluorescent particles [34], and organelles in the cell [35]. Besides, it is free from the limitation on the depth of cell manipulation in the suspensions and does not require any elaborated substrates, providing a flexible platform that can be easily integrated with microfluidics.

In this chapter, we will discuss the multifunctional manipulation of cells with the designed optical fiber probes (FPs). We will show the precise regulation and

bidirectional transport of the cell chain with the FPs. Furthermore, it can also conduct the dynamic rotation and deformation of human red blood cells. With the further combination into the microfluidic technique, FPs have enabled the precise control of cell and further applied into the noninvasive analysis for the endocytosis and extrocytosis behaviors.

3. Optical fiber probe-based manipulation of cells

3.1 The regulation of the cell chain

Figure 1 schematically shows the formation and regulation process of an *E. coli* cell chain. After *E. coli* cells trapped one by one, a cell chain consisted of six *E. colis* was organized at the probe tip. By adjusting FP 2 to approach *E. coli* 5, the cell is rotated and orientated toward the axial direction of FP 2. Then, *E. coli* 5 is removed from the chain with the cell contact sequence changed. By shifting FP 2 along the *+x* direction, *E. coli* 5 is put between the *E. coli* 3 and 4 (**Figure 1c**). After turning off the laser in FP 2, *E. coli* 5 is gradually rotated and orientated along the axial

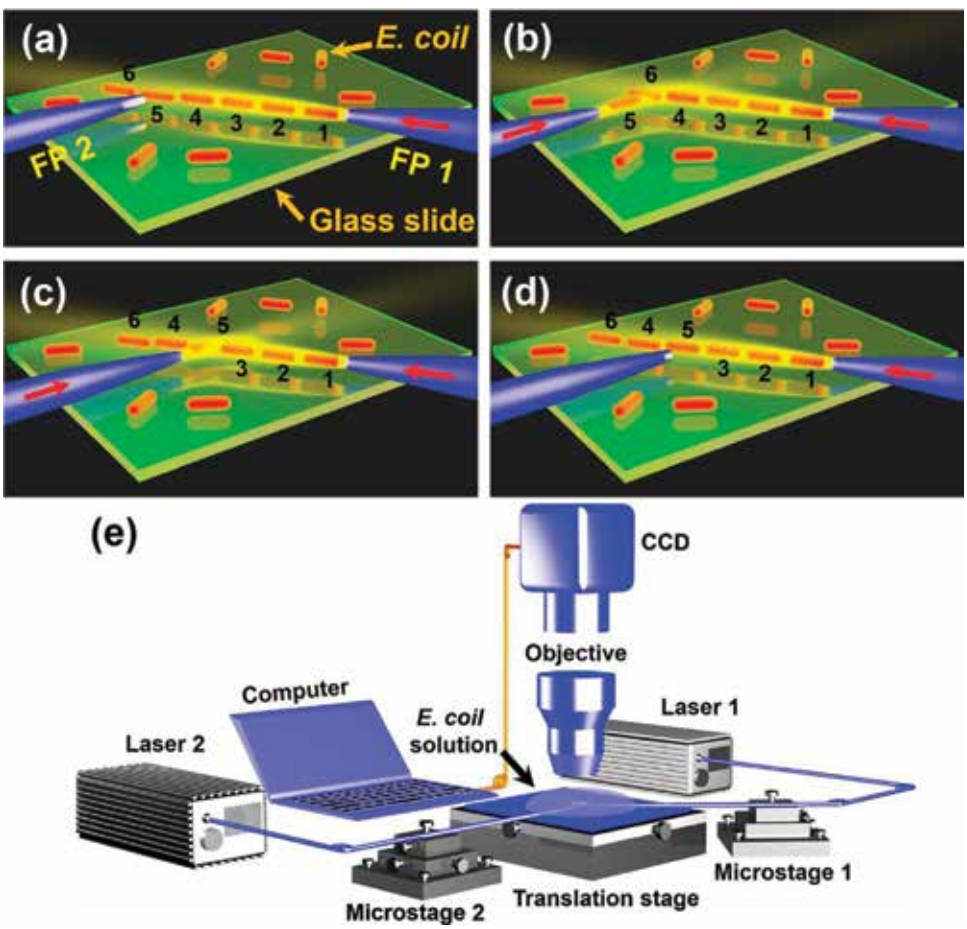

Figure 1.
Schematic of the regulation process and experimental setup. (a) A cell chain is organized at the tip of FP 1. (b) By manipulating FP 2, E. coli 5 is rotated and then removed from the cell chain. (c) E. coli 5 is added back at a new position into the chain. (d) After turning off the laser in FP 2, E. coli 5 is orientated along the axial direction of FP 1. (e) Schematic of the experiment setup [38].

direction of FP 1 (**Figure 1d**), changing the cell contact sequence again. **Figure 1e** schematically shows the experimental setup. After sheathed with a glass capillary, FPs 1 and 2 were fixed on microstages 1 and 2, respectively. The probe tips were immersed in the *E. coli* solution, while their ends were connected to the lasers 1 and 2, respectively. The wavelength of both lasers is set at 980 nm due to the low absorption for the biological cells [36]. Such a wavelength induces little optical damage to bacteria and mammalian cells [37]. The *E. coil* solution was dropped on a glass slide with an injector. The slide was mounted on an *x*–*y* manual translation stage (resolution: 50 nm) to achieve fine positioning and mechanical stability. An optical microscope incorporated with a charged coupled device (CCD) was used for the real time monitoring, image capturing, and video recording.

To demonstrate the operation mechanism, a dynamic regulation of the cell chain was experimentally conducted. After the laser beam injected into FP 1 (P_1 = 30 mW) at t = 0 s, a cell chain was organized at the probe tip, which was consisted of 10 *E. colis*. Then, FP 2 was adjusted to approach the downside tip of *E. coli* 3 (indicated by the yellow dot) in the cell chain (**Figure 2a**). After turning on the laser in FP 2 (P_2 = 50 mW), the downside tip of *E. coli* 3 was trapped by FP 2 (**Figure 2b**). With a shift of 1.9 μm along the –*x* direction, the downside tip was shifted along the –*x* direction, while the upside tip (indicated by the red dot) remained stationary (**Figure 2c**). After that, *E. coil* 3 was rotated clockwise and gradually orientated along the axial direction of FP 2 (**Figure 2d**). Then, it was removed from the cell chain and shifted along the –*x* direction. After that, FP 2

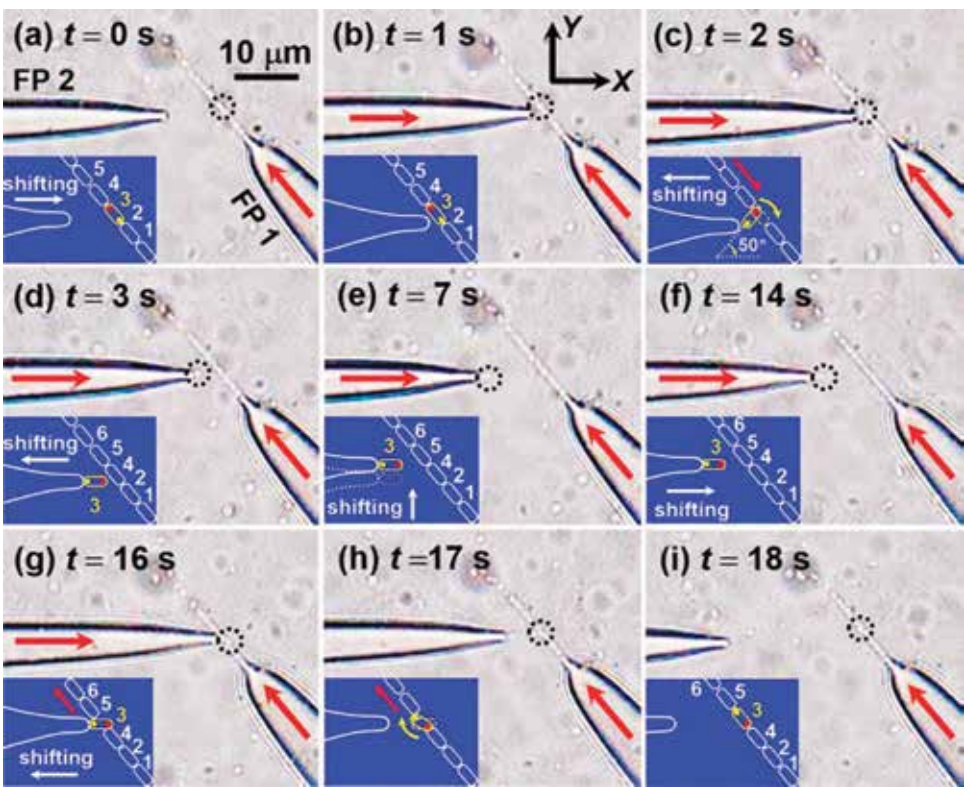

Figure 2.
Optical microscopic images of adjusting the cell contact sequence. (a) FP 2 was adjusted to approach E. coli 3. (b–d) E. coli 3 was rotated and then trapped by FP 2. (e and f) E. coli 3 was shifted with FP 2 along the +y and +x direction. (g–i) The E. coli 3 was added back into the cell chain. The two tips of E. coil 3 were indicated by yellow and red dots [38].

was shifted along the +*y* direction with a distance of ~1 μm (**Figure 2e**), followed by a shift of 9 μm along the +*x* direction (**Figure 2f**). Then, *E. coli* 3 was added back into the chain between *E. coils* 4 and 5 (**Figure 2g**). After the laser off in FP 2, *E. coli* 3 was reorientated along the axial direction of FP 1, and the contact sequence was changed to 1-2-4-3-5-6-7-8-9-10 (**Figure 2h** and **i**).

To quantitatively interpret the above experiment, the optical torques (T) on the *E. colis* were calculated in the regulation process, which is defined as:

$$\boldsymbol{T} = \int \boldsymbol{r}_i \times d\boldsymbol{F}_{EM} \tag{1}$$

where $\boldsymbol{r}_i$ is the position vector pointing from the central point of *E. coli* to the interaction point, $d\mathbf{F}_{EM}$ is the electromagnetic force element exerted on the interaction point i. $\boldsymbol{F}_{EM}$ can be expressed as:

$$\boldsymbol{F}_{EM} = \oint_S (\langle \boldsymbol{T}_M \rangle \cdot \boldsymbol{n}) \mathrm{d}S \tag{2}$$

where dS is the surface element surrounding the cell, $\boldsymbol{n}$ is the surface normal vector, and $\langle \boldsymbol{T}_M \rangle$ is the time-independent Maxwell stress tensor. The optical torque along the +z direction is defined as positive, under which the cell will be rotated counterclockwise. As shown in **Figure 3**, the torques are positive and negative in the regions I ($-50° < \theta < 0°$) and II ($0° < \theta < 50°$). Thus, *E. coli* 3 will be rotated counterclockwise and clockwise, as indicated by the red and blue arrows, respectively. Finally, *E. coli* 3 will be oriented along the axis direction of FP 2, that is, at

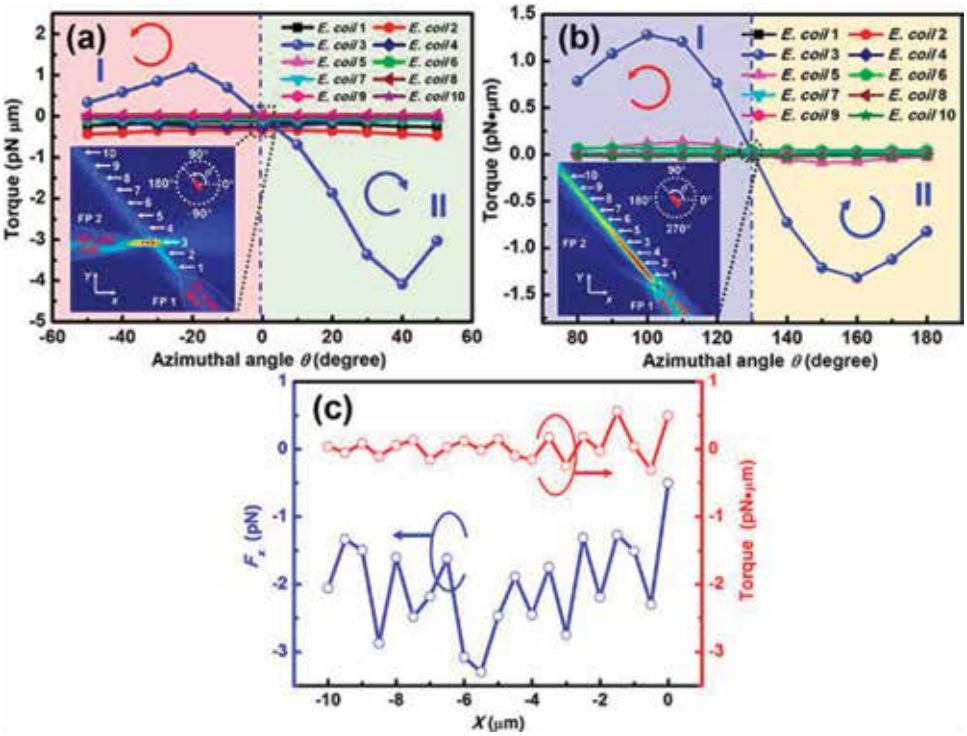

Figure 3.
Calculated optical torque and force during the regulation progress. (a) Calculated optical torque exerted on the 10 E. colis as a function of θ (FP 1: 30 mW and FP 2: 50 mW). The inset shows the energy density distribution at θ = 0°. (b) Calculated optical torque exerted on the 10 E. colis as a function of θ (FP 1: 30 mW and FP 2: 0 mW). The inset shows the energy density distribution at θ = 130°. (c) Calculated optical force F_x and torque on the E. coli 3 as a function of X [38].

θ = 0°. **Figure 3b** shows the torques exerted on *E. colis* after turning off the laser in FP 2. The torques were positive and negative in the region I (80° < θ < 130°) and II (130° < θ < 180°), respectively. At θ = 130°, the torque exerted on *E. coli* 3 was zero so that *E. coli* 3 will be stably trapped and oriented along the axial direction of FP 1. Moreover, during the shift process of FP 2, the optical force and torque exerted on *E. coli* 3 were calculated as shown in **Figure 3c**. During the shift process, the optical force was negative while the torque remained to be zero, indicating *E. coli* 3 will be stably trapped and shifted with FP 2.

Further, the numerical simulations show that the method can be used for the regulation of cell chains consisted of cells with different sizes and shapes (e.g., spherical). After the FPs incorporated into lap-on-chip platforms, the presented regulation method is expected to enable a new opportunity for the investigation of cell growth, intercellular singling pathway, and pathogenic processes.

3.2 Optofluidic organization and transport of the cell chain

Except for the precise regulation, the organized cell chain can also be dynamically transported with an optofluidic strategy, by implanting a large-tapered-angle fiber probe (LTAP) into the microfluidic technique. As shown in **Figure 4a**, when an *E. coli* cell was delivered toward the LTAP tip by the flow, it will suffer from the opposite optical scattering force. The cell kept slowing down until it was trapped stably. Then, *E. colis* were trapped one after another, and a cell chain was organized along the optical axis of LTAP (i.e., x-axis). Further, the distance between the probe tip and cell chain (D) can be dynamically adjusted so that the cell chain can be under bidirectional transportation.

Then, the experiment was conducted to demonstrate the bidirectional transportation of the cell chain (**Figure 4b**). The flow velocity was fixed at V = 10 μm/s, while the laser power (P) was set to be 75 mW. At t = 0 s, a chain consisted of eight cells was organized in front of LTAP at D = 27 μm. After P decreased from 75 to 60, 45, 30, and 15 mW, the chain was transported toward LTAP with D varied from 27 to 22, 17, 10, and 0 μm (**Figure 4b2–6**), respectively. Further, the cell chain can be pushed away from the probe tip by increasing the laser power. As shown in **Figure 4c**, with P increased from 15 to 30, 45, 60, 75, and 90 mW (**Figure 4b2–6**), the cell chain was continuously pushed away from the LTAP tip with D varied from 0 to 10.3, 16.5, 21.4, 26.6 and 32.9 μm, respectively.

In addition, spherical eukaryotes (e.g., yeast cells) can also be organized and transported with the proposed optofluidic technique (**Figure 5a**). The flow velocity and laser power were set to be V = 20 μm/s and P = 40 mW, respectively. First, four yeast cells were trapped and then arranged into a cell chain at t = 0 s. Then the cell chain was transported toward the LTAP tip with V increased to be 32 μm/s. Meanwhile, D was decreased from 23 to 18 μm (**Figure 5a3**). By varying V to 17 and 13 μm/s, the cell chain was further transported with D changed to 25 and 27.5 μm, respectively. Further, the optofluidic transportation of human red blood cells (RBCs) was also conducted to investigate the potential application in the blood diagnose. The flow velocity was fixed at 10 μm/s along the $-x$ direction. Notably, an LTAP tip with a more flat facet was fabricated to ensure the manipulation stability for the larger RBCs (**Figure 5b**). After the laser beam was injected into LTAP (P = 40 mW), two RBCs were transported along the $-x$ direction by the flow and then trapped by the LTAP (**Figure 5b1**). At t = 4, 8, and 12 s, the cell number of the RBC chain was increased from 2 to 3, 4, and 5, respectively. After organizing cell chain, it can be transported by adjusting the laser power. As shown in **Figure 5c**, a cell chain was organized in front of the probe tip. With P increased from 30 to 55 mW, D was also varied from 8.2 to 21.2 and 35.2 μm, as shown in **Figure 5c2** and **c3**, respectively. After that, the chain

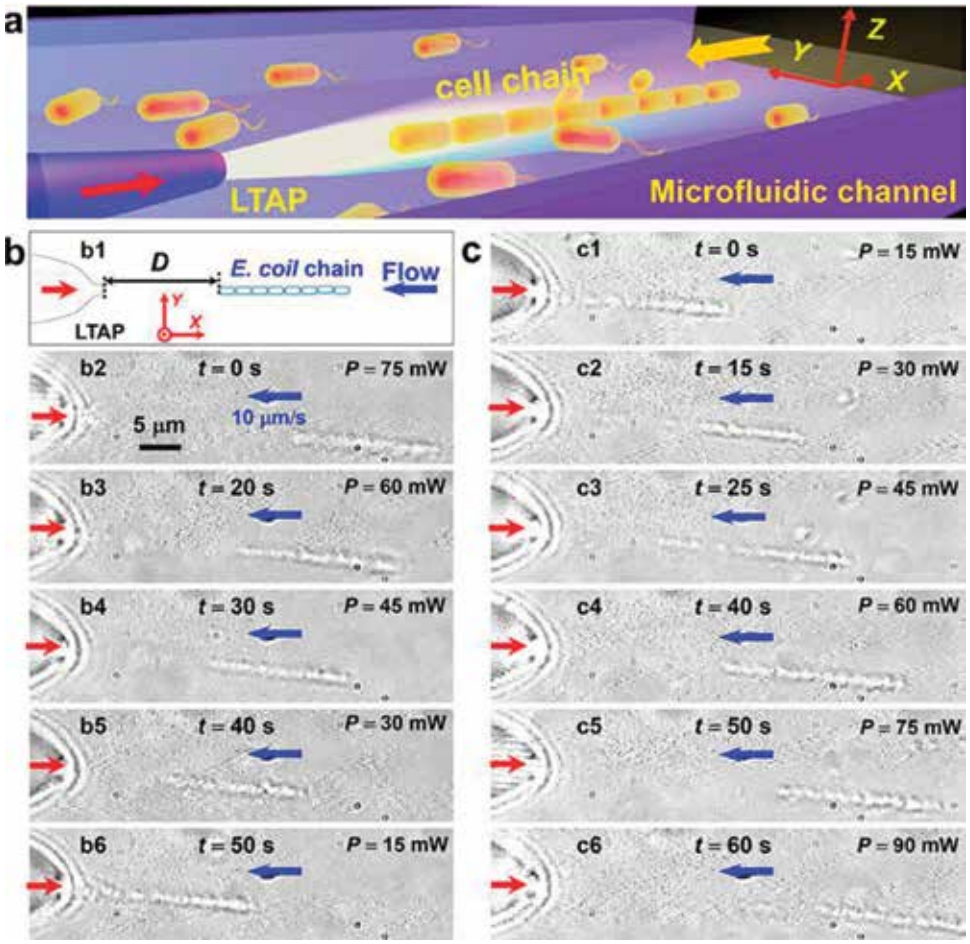

Figure 4.
(a) Schematic of optofluidic organization and transport of cell chain. (b) The cell chain was transported toward the LTAP tip by decreasing the laser power. (c) The cell chain was pushed away from LTAP tip by increasing the laser power [39].

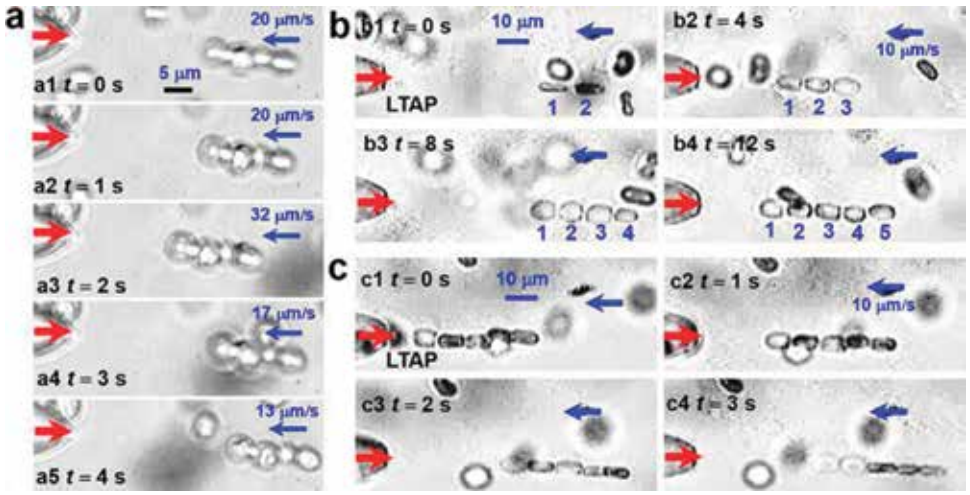

Figure 5.
(a) Optofluidic transport of yeast cell chain under various flow velocities. (b) Optofluidic organization of RBC chain consisted of five red blood cells. (c) Optofluidic transport of the RBC chain [39].

kept stationary with D remained at 35.2 μm (**Figure 5c4**). Besides, the distance can also be changed by adjusting the flow velocity, which was similar to the case of yeast cell chain. These results demonstrated that various cell chains can be dynamically transported by adjusting the laser power or flow velocity.

3.3 Optical rotation and deformation of human red blood cells

Except for the bidirectional transportation of the RBC chain, FPs were also investigated to conduct the multifunctional rotation and deformation of human red blood cells, which were of great physiological and pathological significance. As shown in **Figure 6**, one RBC was bound to the tip of TFP 1 at θ = 0° due to the optical gradient force and the Van der Waals force. At t = 0 s, the laser beam at a wavelength of 980 nm was injected into TFP 2 at P_2 = 24 mW (**Figure 6a1**). Meanwhile, the upper part of the RBC was trapped by TFP 2. By shifting TFP 2 along the $-y$ direction, the cell rotated around the x-axis with θ increased (**Figure 6a2–5**). At t = 10 s, TFP 2 was shifted along the $+y$ direction, and θ decreased to be 0° (**Figure 6a6–10**).

To quantitatively analyze the above rotation process, y_{TFP2} and θ were achieved as shown in **Figure 6b**. In the region I (from t = 0 to 3.8 s), TFP 2 was shifted along the $-y$ direction with a distance of 3.3 μm, and θ increased from 0 to 90°. Then, θ remained to be 90° from 3.8 to 5 s (region II), which indicated a certain orientation of cell can be realized by manipulating TFP 2. After that, θ increased from 90 to 172° (region III) with TFP 2 shifted along the $-y$ direction again, and then it remained to be 172° from t = 7 to 9.5 s (region VI). From t = 9.5 to 15 s, TFP 2 was shifted along the $-y$ direction so that θ decreased from 172 to 0° (region V). Thus, a controllable rotation and orientation of the RBC around x-axis can be realized by manipulating TFP 2. In addition, the shift velocity of TFP 2 (V_{TFP2}) and angular velocity of the RBC (ω_{RBC}) were also calculated. As shown in **Figure 6c**, the value of ω_{RBC} monotonously varied with V_{TFP2}, with a maximum of 4.7 rad/s. Notably, the trapped part can be changed by adjusting TFP 2 along the z direction. For example,

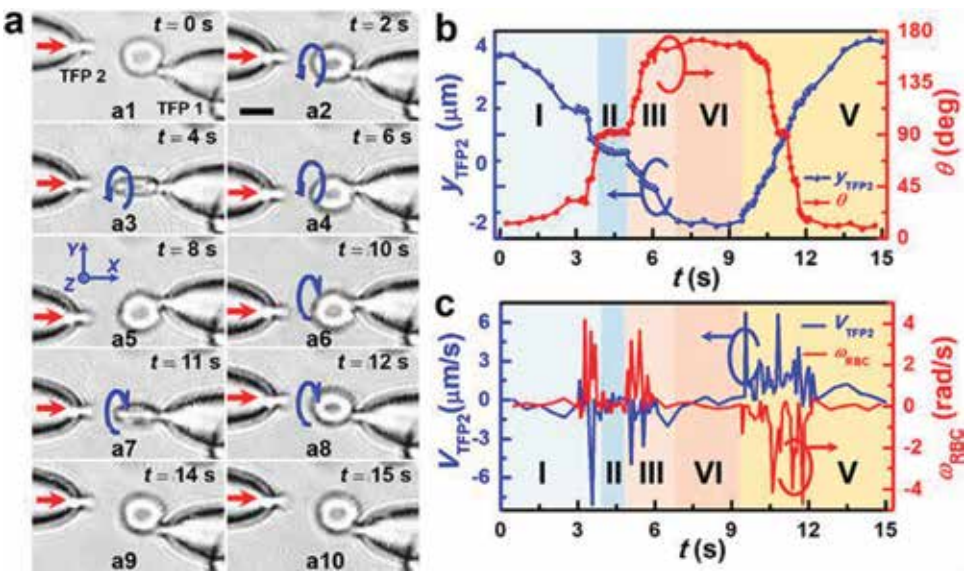

Figure 6.
RBC rotation around x-axis. (a) Optical microscopic images for rotating an RBC around x-axis. Scale bar: 5 μm. (b) Calculated y_{TFP2} and θ in the rotation process. (c) Calculated V_{TFP2} and ω_{RBC} in the rotation process [40].

by trapping the left part of the cell, the cell will rotate around z-axis, which can realize the multifunctional rotation around different axes.

Further, a stretch of single or multiple RBCs can also be realized by using two TFPs. As schematically shown in **Figure 7a**, after the laser beams injected into both TFPs 1 and 2, three RBCs are trapped and then stretched along the optical axis of TFPs. The experiments were then conducted to demonstrate the above stretch mechanism. At t = 0 s, two RBCs were located between two TFPs, with diameters of 5.6 and 6.4 μm, respectively (**Figure 7b1**). Then, two laser beams at the wavelength of 980 nm were injected into the TFPs with the power of $P_1 = P_2$ = 20 mW. After that, the RBCs moved toward each other and finally became contacted due to the optical force (**Figure 7b2**). Meanwhile, they were gradually stretched till reaching an equilibrium at t = 10 s (**Figure 7b3**). The deformation degree of RBCs can be described by the shear strain (γ) which was defined as $\gamma = \Delta l/l$, where Δl and l are the cell stretch length and original length, respectively. At t = 10 s (**Figure 7b3**), the shear strain of two cells reached the maximum of 0.14 and 0.12, respectively. Then, they kept stretched until the laser was turned off at t = 35 s (**Figure 7b4**). After that, the RBCs were gradually resumed their original shapes (**Figure 7b5, 6**).

Similarly, the simultaneous stretch of three RBCs was also conducted, as shown in **Figure 7c**. The diameters of RBCs 1, 2, and 3 were 6.7, 5.7, and 6.9 μm, respectively. At t = 2 s, the RBCs began to be trapped and then stretched after the laser turned on (**Figure 7c2**). Meanwhile, the distance between the cells was decreased, while γ were increased. They gradually became contacted with each other. At t = 5 s,

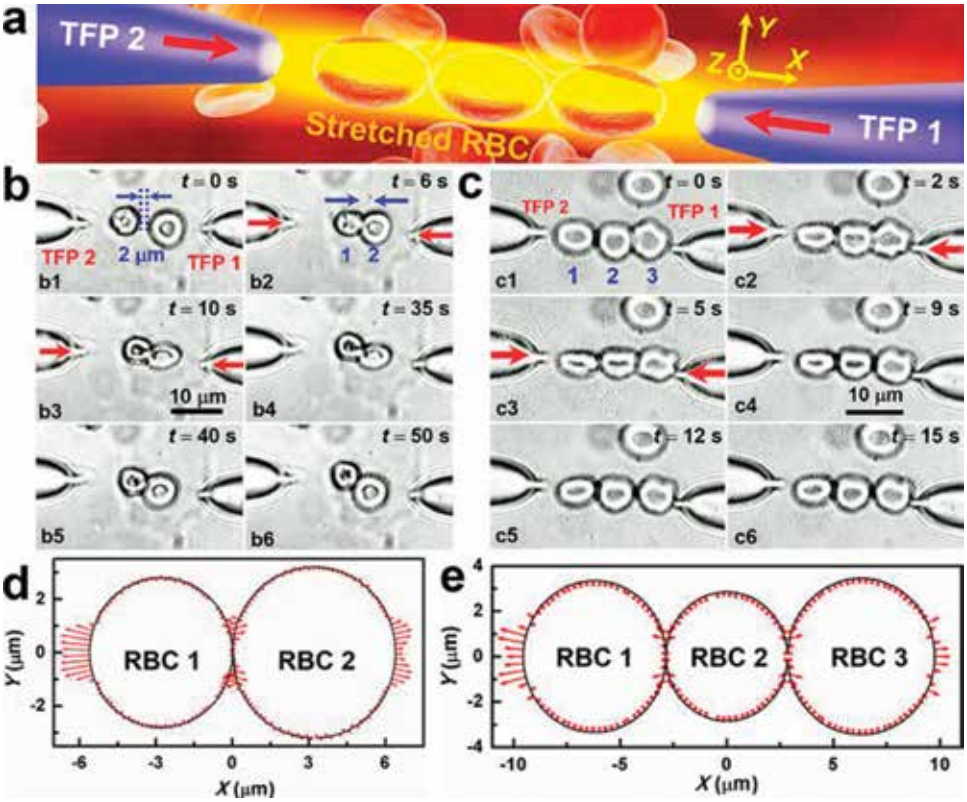

Figure 7.
The stretch of multiple RBCs with light from two TFPs. (a) Schematic of stretching multiple RBCs with two TFPs. (b) Optical microscopic images of stretching two RBCs. (c) Optical microscopic images of stretching three RBCs. (d) Stress distribution on the surfaces of two RBCs. (e) Stress distribution on the surfaces of three RBCs [40].

the three cells reached the equilibrium with γ = 0.15, 0.1, and 0.12 (**Figure 7c3**). After that, RBCs started to resume their original shapes by turning off the laser at t = 9 s (**Figure 7c4–6**). Further, the normalized stress distribution on the RBC surfaces was also investigated, as indicated by the red arrows in **Figure 7e** and **f**. The stress was mainly distributed along the x-axis, and the stress direction was toward the outside of cells. Therefore, the RBCs were stretched and further became contacted with each other.

4. Discussion

From the above analysis, it can be seen that the multifunctional trap and manipulation can be conducted with the fiber probe-based optical tweezers. As we know, a precise control of cell behavior was essential in the research of the endocytosis and exocytosis process, especially for nanomedicine injection, intracellular signaling pathway, and pathogenic progress. After cells manipulated in a controlled manner, various microparticles or viruses can be brought into contact with the targeted cells at specific well-defined time points and positions. Meanwhile, the spatiotemporal effect can be quantitatively investigated of different extracellular cues on the endocytosis and exocytosis process.

Then the potential application and advantages were discussed for fiber probe-based tweezers on the endocytosis and exocytosis purpose. As for the nanomedicine injection, the cells can be located at a different distance to the medicine with the assistance of fiber probes, providing a great way to study the diffusion and transportation process. Further, the nanomedicine can be adjusted to approach various sites of the cell membrane. Then, the endocytosis efficiency on the interaction sites can be quantitatively investigated. Meanwhile, various nanomedicines can approach the targeted cell simultaneously with controlled sites, providing an insight into the study of selective phagocytosis progress. While for the intracellular signaling pathway, spatial manipulation will be beneficial to analyze the effect of contact distance on the cell interaction. As we know, the cell can interact with each other through the exchange of soluble signaling molecules or direct cell-cell contact, which can vary in both time and space continuously. Thus, it is of great importance in dynamically adjusting the cell-cell interaction distance and contact sequence, which can be conducted by using the fiber-probe tweezers. Further, the detailed pathway for the intracellular signaling can be individually investigated with the proposed technique. Besides, in the pathogenic progress, the specific infection site can be decided by using fiber probes to manipulate pathogenic bacterium and targeted cell simultaneously. Thus, the dependence of the contact site on the infection performance can be investigated, which opens up the possibility for analyzing pathogenic dynamics not accessible through passive observation.

5. Conclusions

In this chapter, the fiber probe has been demonstrated to conduct the multifunctional manipulation of cell chains, including the sequential organization, precise regulation, and bidirectional transportation. Besides, the dynamic rotation and deformation of the human red blood cell were also realized using the fiber probes. With the advantage of ease integration, high flexibility, and noninvasive, the proposed technique can provide a great perspective in the investigation of the endocytosis and exocytosis purpose. The targeted cells and pathogenic bacterium can be dynamically manipulated simultaneously, which is anticipated to be useful in

the analysis, diagnosis, and treatment of cell diseases. By incorporating the FPs into lap-on-chip platforms, the presented technique is expected to enable a new opportunity for the investigation of the nanomedicine injection, intracellular signaling pathway, and pathogenic process.

Acknowledgements

This work was supported by the National Natural Science Foundation of China (No. 11774135, 11874183, and 61827822), the Tip-top Scientific and Technical Innovative Youth Talents of Guangdong Special Support Program (No. 2015TQ01X267), the Fundamental Research Funds for the Central Universities (No. 21618301), and the PhD Start-up Fund of Natural Science Foundation of Guangdong Province (No. 2018A030310501).

Conflict of interest

The authors declare no competing financial interests.

Author details

Xiaoshuai Liu and Yao Zhang*
Institute of Nanophotonics, Jinan University, Guangzhou, China

*Address all correspondence to: zhyao5@jnu.edu.cn